Migration velocity analysis by the common image cube analysis (CICA)

Saleh M. Al-Saleh, Gary F. Margrave, Hugh D. Geiger, and John C. Bancroft

ABSTRACT

Wavefield extrapolation methods are powerful for handling strong lateral velocity variations. However, they require an accurate velocity model to produce good images. There are many different migration velocity methods; but most of them make some simplifying assumptions about the subsurface, which reduces their ability to exploit the power of wavefield extrapolation methods.

In this report, we reformulate some well-known migration velocity methods, like residual curvature analysis (RCA), depth focusing analysis (DFA), and common focus point (CFP) analysis into mathematical hypotheses. This reformulation puts them in the same context, so they are easier to understand and compare. Further, by restating the methods as mathematical hypotheses, they are easier to relate to other disciplines such as mathematics and physics.

We also combine different aspects of the RCA, DFA, and CFP methods into a new migration velocity analysis approach called the common image cube analysis (CICA). Instead of simply taking the zero-lag crosscorrelation at each depth level, we store all the crosscorrelation lags. The result is a cube that contains more prestack information than the other methods. Slicing this cube at different lags forms a series of common image gathers (CIGs), where the conventional CIG can be obtained by slicing the cube at the zero lag.

When the background velocity model used for migration is different from the true velocity model, the best-focused CIG is not at zero lag. Searching the cube at other lags for the most focused CIG gives the traveltime shift that is needed to approximately equalize the traveltimes of the upgoing and downgoing wavefields. From the updated traveltimes, the true velocity can be estimated. This approach is tested on models with constant velocity as well as velocity varying with depth, and the results show that it can be used to yield an accurate estimate of the true velocity when the wrong velocity model is used for migration.

INTRODUCTION

Wavefield extrapolation methods are more powerful than the ray-based methods in handling strong lateral velocity variations. Wavefield extrapolation methods are also very sensitive to the velocity models (Berkhout, 1982; Yilmaz and Chambers, 1984; Claerbout, 1985; Al-Yahya, 1989; Deregowski, 1990; Liu and Bleistein, 1994; Varela et al., 1998). Using inaccurate velocity models in wavefield extrapolation methods can generate low quality images. The sensitivity of wavefield extrapolation methods makes them a good tool for velocity analysis.

There are different methods for migration velocity analysis (MVA). One of oldest

methods is the depth focusing analysis (DFA) (Yilmaz and Chambers, 1984; Faye and Jeannot, 1986), which analyzes the energy build-up at the zero offset (source-receiver offset) in a depth focusing panel. In DFA, a migration velocity is acceptable if the difference between the focusing and migration depths is zero. In the literature, the DFA is described and constructed on the basis of shot-geophone migration (the survey sinking concept (Claerbout, 1985). In this method of migration, all the shot gathers are extrapolated to a depth level, and then sorted into receiver gathers, which are downward extrapolated to the same depth level. The reflectivity image at this depth level can be extracted by applying the zero-time and zero-offset imaging conditions. In DFA, the zero-time imaging condition is relaxed and only the zero-offset imaging condition is invoked. Storing this zero-offset trace for all depth levels forms a panel for a specific lateral position. The equivalent procedure in a source profile migration is to downward continue all the shot gathers to a depth level, and then to forward model all the sources to the same depth level. We sort the downward extrapolated shots (upgoing wavefield or the data) for a lateral position and we do the same thing to the modeled sources (downgoing wavefield). The result is two gathers for each lateral position for each depth level. The two gathers are cross-correlated and the result is stacked over offset to give one trace at each lateral position for each depth level. The value at zero-lag of all such traces for all lateral positions and all depths forms the final reflectivity image. Storing this trace at each depth level creates a focusing panel for a specific lateral position. This is consistent with the Berkhout (2001) description of DFA as a double focusing method. The first focusing occurs when extrapolating the data to this depth level and the second occurs when stacking all the offsets. Any traveltime information about the upgoing and downgoing wavefields at the subsurface grid point is lost. Most inversion formulas for the DFA analysis make simplifying assumption about the subsurface and they may fail in the presence of strong lateral velocity variations or steep dips.

The residual curvature analysis method (RCA) (Al-Yahya, 1989) is another MVA method. After prestack migration of common source, receiver, or offset gathers, the imaged multichannel data are sorted into common image gathers (CIGs). The data in each common image gather have the same imaged horizontal location. RCA analyzes the curvatures on the common image gathers (CIGs), where the migration velocity is acceptable if the difference between imaged depths from different offsets is minimal. Inversion formulas are available to analyze the residual moveout on the CIGs and invert for the true velocity (e.g. Lee and Zhang, 1992; Liu and Bleistein, 1994). Most of the inversion formulas are derived based on small offset and smooth lateral velocity variations. Under these assumptions, the estimated velocities may be a good approximation to RMS velocities, so that the estimated velocities can be converted into interval velocities using the Dix equation or other similar formulas (Liu and Bleistein, 1994). In the presence of strong lateral velocity variations, these estimated velocities may differ significantly from the RMS velocities (Lynn and Claerbout, 1982; Liu and Bleistein, 1992). As a result, the velocity-updating procedure may not converge to the correct velocity model.

The common focus point (CFP) analysis (Berkhout, 1997.a; Berkhout, 1997.b) is similar to DFA but it only involves a single focusing where the data are extrapolated to an initial guess of the reflector depth**.** Then the downward extrapolated shots (upgoing wavefield or the data) and the modeled sources (downgoing wavefield) are sorted for a lateral position to form two gathers. In the CFP approach, the background velocity model is acceptable if the traveltimes of two events in these gathers are equal at the initial guess of the reflector. The CFP approach uses the differential time shift (DTS) panel as a tool to test the principle of equal traveltimes. The DTS is formed by crosscorrelating the two gathers, which generates another event in this panel (Berkhout, 1997.b; Berkhout, 2001). Using a correct velocity model will result in a flat event at the zero-lag in the DTS panel. Note that the values at the zero-lag of the DTS panel give the same values in the CIG of the same lateral position at the depth of the initial guess of the reflector. Furthermore, stacking all the traces in the DTS panel over offset produces the same trace that goes into the DFA panel.

Although these methods may seem different from each other, they all are related. However, each method lacks some worthwhile features of the others. For example, in DFA we do not use the CIGs and in CFP we do not use the focusing depth. We propose the common image cube analysis (CICA) migration velocity analysis method, which combines different aspects from existing methods into a more general approach. Instead of retaining only the zero-lag value at each depth level, we store all the lags and form an image cube for a velocity analysis location. The three dimensions of this cube are depth, offset, and lag.

Next we present a brief description of prestack migration of individual source records in order to explain our notation, which is essential for a precise description of the various methods. Then we describe RCA, DFA, and CFP from a mathematical perspective and state them as hypotheses. Next, we introduce the theory of CICA and state the corresponding imaging hypothesis. Simple numerical examples with velocity models that are either constant or depth variant are then used to show that CICA can be used to approximate the true velocity model. The reasons for using simple models in our tests are two fold: (1) they better illustrate the concept behind this approach and (2) for dipping events in a constant velocity medium with large perturbations, CICA can give an accurate estimate of the true velocity while the other approaches need a couple of iterations to achieve an accurate estimate.

SHOT PROFILE MIGRATION USING EXPLICIT WAVEFIELD EXTRAPOLATORS

In shot profile migration, the upgoing and downgoing wavefields are extrapolated separately. Wavefield extrapolation can be done in the $\omega - x$ domain as a nonstationary convolution between the input wavefield using a table of extrapolators, where for each output point a potentially different operator is used (Holberg, 1988; Hale, 1991; Margrave et. al., 2005; Al-Saleh and Margrave, 2005). We assume that a background velocity model, $V_m(x,z)$, is available to define the extrapolation operators. The 2D downward-extrapolated, upgoing wavefield, $U^-(x_s,x,n\Delta z,\omega;V_m)$ is given by

$$U^{-}\left(x_s, x, n\Delta z, \omega; V_m\right) = \left[\left(\prod_{k=1}^{n} L_{k\Delta z}\left(V_m\right)\right) U_o^{-}\right]\left(x_s, x, n\Delta z, \omega\right), \tag{1}$$

where s is an integer shot index ranging from 1 to N (number of shots), Δz is the depth step, x is the transverse coordinate, x_s is the shot coordinate, ω is the temporal frequency, and k is an integer such that $k\Delta z$ gives a particular depth, n is positive integer such that $n\Delta z$ gives the maximum depth of interest, U_o^{-} is the Fourier transform over the temporal coordinate of the recorded wavefield at the surface, and the cascade of wavefield extrapolation operators $L_{k\Delta z}\left(V_m\right)$ is described by

$$\prod_{k=1}^{n} L_{k\Delta z}\left(V_m\right) = L_{n\Delta z}\left(V_m\right) \circ L_{(n-1)\Delta z}\left(V_m\right) \circ \ldots\ldots\ldots L_{\Delta z}\left(V_m\right). \tag{2}$$

In this expression $L_{k\Delta z}\left(V_m\right)$ means an operator that depends upon $V_m\left(x, z\right)$ but operates on a wavefield, and $\circ$ denotes operator composition. In a one-way, primaries only, wavefield extrapolation, the k^{th} operator depends only upon that part of $V_m\left(x, z\right)$ in the interval $z \in \left[\left(k-1\right)\Delta z, k\Delta z\right]$. The recorded wavefield at the surface is described by

$$U_o^{-} = U^{-}\left(x_s, x, 0, \omega\right). \tag{3}$$

Applying the first operator to the recorded or upgoing wavefield can be described by

$$\left(L_{1\Delta z}\left(V_m\right) U_o^{-}\right)\left(x_s, x, \Delta z, \omega\right) = \frac{1}{2\pi}\int_{\mathbb{R}} U^{-}\left(x_s, x', 0, \omega\right) W_{k=1}\left(x - x', x, \omega\right) dx' \tag{4}$$

where

$$W_k\left(x - x', x, \omega\right) = \frac{1}{2\pi}\int_{\mathbb{R}} \hat{W}_k\left(k_x, x, \omega\right) \exp\left(ik_x\left(x - x'\right)\right) dk_x, \tag{5}$$

$$\hat{W}_k\left(k_x, x, \omega\right) = \exp\left(ik_z\left(\omega, k_x, x\right)\Delta z\right), \tag{6}$$

and

$$k_z\left(\omega, k_x, x\right) = \begin{cases} \sqrt{\dfrac{\omega^2}{V_k\left(x\right)^2} - k_x^2}, & \dfrac{\omega^2}{V_k\left(x\right)^2} > k_x^2 \\ i\sqrt{k_x^2 - \dfrac{\omega^2}{V_k\left(x\right)^2}}, & \dfrac{\omega^2}{V_k\left(x\right)^2} \le k_x^2 \end{cases}. \tag{7}$$

Also in equation (7) $V_k\left(x\right)$ is some appropriate average of $V_m\left(x, z\right)$ over $z \in \left[\left(k-1\right)\Delta z, k\Delta z\right]$. Similarly, the forward-modeled source, or downgoing wavefield, $D^{+}\left(x_s, x, n\Delta z, \omega; V_m\right)$, is given by

$$D^+\left(x_s,x,n\Delta z,\omega;V_m\right)=\left[\left(\prod_{k=1}^{n}L^*_{k\Delta z}\left(V_m\right)\right)D_o^+\right]\left(x_s,x,n\Delta z,\omega\right), \tag{8}$$

where '*' indicates the complex conjugate. Equation (8) expands to

$$D^+\left(x_s,x,n\Delta z,\omega;V_m\right)=L^*_{n\Delta z}\left(V_m\right)\circ L^*_{(n-1)\Delta z}\left(V_m\right)\circ .....L^*_{\Delta z}\left(V_m\right)D_o^+ \tag{9}$$

where

$$D_o^+=D^+\left(x_s,x,0,\omega\right) \tag{10}$$

and

$$L^*_{\Delta z}\left(V_m\right)D_o^+=\frac{1}{2\pi}\int_{\mathbb{R}}D^+\left(x_s,x',0,\omega\right)W^*_{k=1}\left(x-x',x,\omega\right)dx'. \tag{11}$$

So the downward-extrapolated upgoing and forward-modeled downgoing wavefields to a depth level *z* can be obtained by applying a cascade of operators (equations (1) and (8)). Equations (4) and (11) are equivalent to the generalized phase-shift-plus-interpolation (GPSPI) method (Margrave and Ferguson, 1999), which is the limiting form of PSPI (Gazdag and Squazerro, 1984). However, W that is used in the equations above is not compactly supported. In fact it is known to be a first-order Hankel function of the first kind (multiplied by a simple scalar). There are different methods that can be used to design stable, compactly supported operators that can be used in a similar fashion to equations (4) and (11). In this report, we will use the enhanced forward operator and conjugate inverse (FOCI) algorithm to perform the shot profile migration (Margrave et al., 2005; Al-Saleh and Margrave, 2005). Using the FOCI approximation to W instead of the exact kernel in equations (4) and (11) is a highly accurate approximation to GPSPI.

RCA APPROACH

A stacked section, or reflectivity image, from 2D prestack depth migration may be obtained by applying the cross-correlation imaging condition (Claerbout, 1985) and summing over all the shots

$$I\left(x_o,z;V_m\right)=\sum_s\int_{\mathbb{R}}U^-\left(x_s,x_o,z,\omega;V_m\right)D^{+*}\left(x_s,x_o,z,\omega;V_m\right)d\omega \tag{12}$$

where we denote a specific inline coordinate by x_0 and have set $z=n\Delta z$. $I\left(x_o,z;V_m\right)$ does not have any prestack information, meaning that it only shows the average reflectivity as seen over the available incidence angles at any point in (*x*,z) (de Bruin et. al., 1990). One way to get prestack information is to use a common image gather (G_{ci}) defined as

$$G_{ci}\left(x_s, x_o, z; V_m\right) = \int_{\mathbb{R}} U^{-}\left(x_s, x_o, z, \omega; V_m\right) D^{+*}\left(x_s, x_o, z, \omega; V_m\right) e^{i\omega(\tau=0)} d\omega \qquad (13)$$

In equation (13) we explicitly note that only the zero-lag value $(\tau = 0)$ has been used. The following hypothesis describes the basics of residual curvature analysis (RCA) that uses the CIGs. We use the term *background velocity model* to describe the velocity field used for the imaging process that creates the CIGs; and *image depth* will refer to the depth at which a reflector appears in the imaging process. Generally, the background velocity model will resemble but not equal the true velocity field. The image depth will approach the true reflector depth when the background model approaches the true field. We will also make the trivial coordinate transformation in each CIG from source coordinates to offset coordinates defined by $x_h = x_s - x_0$. Thus we label each trace in a CIG by the lateral distance (offset) from the image point, x_0, to the surface source location, x_s.

The RCA imaging hypothesis: *A velocity model is correct when reflection events in the CIG's are essentially invariant with offset (flat).*

For a 2D dataset of *N* shots, having a maximum temporal signal frequency of $f_{\max} = (2\pi)^{-1}\omega_{\max}$, and a prestack depth migration resulting in a set of common image gathers ($G_{ci}\left(x_h, x_0, z; V_m\right)$) using a background velocity model, V_m, let a reflection event in a specific common image gather at lateral position x_0 be identified with the trajectory $z_e\left(x_h\right)$ with offset coordinates $x_h = x_s - x_0$ ranging from x_α to x_β. That is $G_{ci}\left(x_h, x_0, z = z_e\left(x_h\right); V_m\right)$ is identified with the reflection event. Then we will say that V_m is correct to δ wavelengths, and write $V_m =_\delta V$, for lateral position x_0 and image depth $\overline{z}$ if there exists a dimensionless number $\delta > 0$ such that

$$\left\| z_e\left(x_s\right) - \overline{z} \right\|_2 \le \delta \lambda_{\min}, \qquad (14)$$

where $\| \ \|_2$ denotes the L_2 norm and

$$\overline{z} = \text{mean}\left(z_e\left(x_h\right)\right), \ \ x_h \in \left[x_\alpha, x_\beta\right] \qquad (15)$$

and

$$\lambda_{\min} = \frac{V_m\left(x_0, \overline{z}\right)}{f_{\max}}. \qquad (16)$$

■

In other words, when using a background velocity model that resembles the true velocity field, the event, $z_e\left(x_h\right)$, will appear as a flat event (i.e. nearly constant depth) on the CIG and a smile or frown otherwise (Zhu et. al., 1998). There are many inversion

formulas that analyze the residual moveout on the CIGs to invert for a velocity model that approximates the true velocity field (Lee and Zhang, 1992; Liu and Bleistein, 1994). The problems with these inversion formulas are two fold: (1) most of them are derived based on small offset and smooth lateral velocity variations and (2) the difference between the background velocity and true velocity field is small. If these assumptions are not valid then RCA might fail to approximate the true velocity field.

DFA APPROACH

In the depth focusing analysis (DFA), the zero-lag imaging condition is relaxed and the offsets are stacked to give one trace. To facilitate this, we generalize the CIG definition of equation 13 to define depth focusing gathers as

$$G_{df}\left(x_h, x_o, z, \tau; V_m\right) = \int_{\mathbb{R}} U^{-}\left(x_s, x_o, z, \omega; V_m\right) D^{+*}\left(x_s, x_o, z, \omega; V_m\right) e^{i\omega\tau} d\omega \qquad (17)$$

which simply generalizes equation (13) to non-zero lag. Here again $x_h = x_s - x_0$. Thus $G_{df}\left(\tau = 0\right) = G_{ci}$.

The basics of DFA can be described using the following hypothesis.

DFA imaging hypothesis: *A velocity model is correct when the maximum stacked power of the depth focusing gathers occurs at zero lag.*

For a 2D dataset of N shots, having a maximum temporal signal frequency of $f_{\max} = (2\pi)^{-1}\omega_{\max}$, and a prestack depth migration resulting in a set of depth focusing gathers ($G_{df}\left(x_h, x_o, z, \tau; V_m\right)$) using a background velocity model, V_m, let the gathers be stacked over offset to define the stacked power function

$$\sigma\left(x_0, z, \tau; V_m\right) = \left\| \sum_{x_h} G_{df}\left(x_h, x_0, z, \tau; V_m\right) \right\|_2^2 \qquad (18)$$

and then define the lag, τ_0, of the peak power by

$$\sigma\left(x_0, z, \tau_0; V_m\right) = \max_{\tau}\left[\sigma\left(x_0, z, \tau; V_m\right)\right] \qquad (19)$$

We say that a reflector exists at every depth for which a distinct maximum can be found.

Then, for a fixed depth $z = z_f$ called the focusing depth, we say the velocity model is correct to ε periods, and write $V_m =_{\varepsilon} V$, if there exists an $\varepsilon > 0$ such that

$$\tau_0 f_{\max} < \varepsilon . \qquad (20)$$

As $\varepsilon \to 0$ the focusing depth is assumed to approach the true reflector depth.

■

DFA uses the stacked power to measure the velocity error. Most inversion formulas for the DFA analysis make simplifying assumptions about the subsurface and they may fail in the presence of strong lateral velocity variations and steep dips. Further, it might be difficult to find the focusing depth due to spurious focusing (MacKay and Abma, 1993).

CFP APPROACH

By looking at upgoing and downgoing wavefields before invoking the imaging condition, we can have two gathers in the time domain. The downward-extrapolated, time-domain, upgoing wavefield is given by

$$u^-(x_s,x,z,t;V_m)=\frac{1}{2\pi}\int_{\mathbb{R}}U^-(x_s,x,z,\omega;V_m)e^{i\omega t}d\omega \tag{21}$$

and the forward-modeled, time-domain, downgoing wavefield is given by

$$d^+(x_s,x,z,t;V_m)=\frac{1}{2\pi}\int_{\mathbb{R}}D^+(x_s,x,z,\omega;V_m)e^{i\omega t}d\omega \tag{22}$$

The following hypothesis describes some basics of the CFP approach.

The CFP imaging hypothesis: *The velocity model is correct when the downgoing wavefield matches an event in the upgoing wavefield.*

As in DFA, a 2D dataset of *N* shots, having a maximum temporal signal frequency of $f_{\max}=(2\pi)^{-1}\omega_{\max}$, is passed into a prestack depth migration, using a background velocity model, V_m, and with a pre-selected set of depth locations, (x_0,z_i), $i\in[1,2,\cdots M]$. At each of these locations we estimate separately the upgoing time-domain wavefield, $u^-(x_h,x_o,z_i,t;V_m)\equiv u_i^-(x_h,t;V_m)$, and its downgoing sibling $d^+(x_h,x_{oi},z_i,t;V_m)\equiv d_i^+(x_h,t;V_m)$. Unlike DFA, we do not form the G_{df} explicitly and we do not stack over offset. At each of the *M* analysis locations, a reflection event is picked on the $u_i^-(x_h,t;V_m)$ and its corresponding downgoing wave is picked on $d_i^+(x_h,t;V_m)$. If the velocity model is exactly correct, these two events will occur on precisely the same time-offset function $t_i(x_h)$; however, in general, we will have a function $t_{ui}(x_h)$ on the upgoing wave and a different traveltime function $t_{di}(x_h)\neq t_{ui}(x_h)$ on the downgoing wave. The difference between these defines an offset-variant lag function $\tau_i(x_h)=t_{ui}(x_h)-t_{di}(x_h)$, which we will call the depth-specific delay function, which is the fundamental measure of the velocity model mismatch that is provided by CFP. These delay functions can be obtained directly by crosscorrelating $u_i^-(x_h,t;V_m)$ with $d_i^+(x_h,t;V_m)$ and picking the location of maximum absolute value of the crosscorrelation function on each trace. In fact, the crosscorrelation of $u_i^-(x_h,t;V_m)$ with $d_i^+(x_h,t;V_m)$ is called the *differential time shift panel* or DTS panel

and is a common tool. Since the G_{df} are just such crosscorrelations at all depths then the DTS is simply a constant depth slice of the G_{df}. The analysis of the G_{df} as a cube in (x_h, x_0, z), as we will shortly describe, is not typically carried out.

We say that V_m is correct to ε periods, and write $V_m =_\varepsilon V$, at a position (x_0, z_i) if there exists a nonnegative, dimensionless number ε such that

$$\left|\tau_i(x_h)\right| f_{\max} < \varepsilon, \ \forall x_h \in \left[x_\alpha, x_\beta\right], \tag{23}$$

■

The CFP approach is based on the principle of equal traveltime of events in the upgoing and downgoing wavefields (Berkhout, 1997.b), which states that if the velocity model is correct then the traveltime function, $t_d(x_h, x_0, z_r)$, of the first arrival of the downgoing field will match the traveltime function, $t_u(x_h, x_0, z_r)$, of a particular reflection at the reflector depth, z_r. In essence, this is simply a restatement of Claerbout's imaging principle (Claerbout, 1976) which states that a reflector exists in the subsurface where the upgoing and downgoing wavefields are coincident in time. While it is clear that a correct velocity model will have this property for a number of reflection events, it is not necessarily true that a model which satisfies this principle for a finite number of reflection events is close to the correct model. In other words, this is a necessary condition but not, in general, sufficient.

CFP analysis is similar to DFA in that, in principle, both create and analyze the gathers $G_{df}(x_h, x_o, z, \tau; V_m)$ specified by equation (17). Although CFP does not explicitly form these gathers, an equivalent process could do so. DFA analyzes these gathers by the simple expedient of stacking over offset and looking for power maxima. The result is just a single bulk estimate of a traveltime mismatch at each (x_0, z). In contrast, CFP analyzes the data over offset without stacking and thereby, with greater effort, obtains estimates of traveltime mismatches as a function of offset for each analysis location. The CFP information set is much richer than DFA and offers more potential for inversion to estimate the appropriate velocity model updates.

By splitting $\tau_i(x_h)$ and applying half of it to the upgoing field and half to the downgoing field (as simple offset dependent time shifts), the velocity can be inverted from the updated traveltimes. The depth-specific delay functions for a good migration velocity model should all satisfy $\left|\tau_i(x_h)\right| f_{\max} < \varepsilon, \forall x_h \in \left[x_\alpha, x_\beta\right]$ for some $\varepsilon < 1$. The criterion $\forall x_h \in \left[x_\alpha, x_\beta\right]$ is not mentioned in the original description of the CFP approach by Berkhout (1997.b).

Figure 1 shows an example of CFP gathers. In this particular example, $z_i = z_r$ and $V_m =_\varepsilon V$. Figure 1.a shows the final stacked section obtained with the correct

velocity and the analysis location (dashed line). Figures 1.b and 1.c show the upgoing, $u^{-}(x_h, x_0, z_r, t)$ and downgoing wavefields, $d^{+}(x_h, x_0, z_r, t)$ where $x_0 = 1000\,\text{m}$ in this particular example. Figure 1.d shows the DTS panel where $|\tau_i(x_h)|\, f_{\max} < \varepsilon$. Note also that when using $V_m =_{\varepsilon} V$, the depth-specific delay function, $\tau_i(x_h)$, should have no dependence on offset at the reflector depth. These figures show that when $V_m =_{\varepsilon} V$, the extrapolated upgoing and downgoing wavefields at the reflector depth should have the same traveltime, which also means that, $\tau(x_h, x_0, z_r)$ is zero. Note that in this example there is only one event in each gather.

THE COMMON IMAGE CUBE ANALYSIS APPROACH (CICA)

We propose a method that combines some aspects of the RCA, DFA, and CFP methods. The following hypothesis describes this method.

The CICA imaging hypothesis: *The velocity model must meet the RCA, DFA, and CFP criteria to be correct. It can be most easily assessed and updated by analyzing the entire* G_{df} *cube at selected analysis location.*

As in DFA and CFP, a 2D dataset of *N* shots, having a maximum temporal signal frequency of $f_{\max} = (2\pi)^{-1}\omega_{\max}$, is passed into a prestack depth migration, using a background velocity model, V_m, and resulting in a set of depth focusing gathers, $G_{df}(x_h, x_o, z, \tau; V_m)$. Unlike DFA and CFP, we now analyze the G_{df} without stacking at a fixed lateral position and at all depths (x_0, z). Let a reflection event in a specific depth focusing gather obtained at some specific τ at lateral position x_0 be identified with the surface $z_e(x_h, \tau)$ with offset coordinates $x_h = x_s - x_0$. Typically, this event will correspond to a set of local crosscorrelation maxima in the sense that

$$\left|G_{df}(x_h, x_0, z_e(x_h, \tau), \tau; V_m)\right| = \max_{loc}\left(\left|G_{df}(x_h, x_0, z, \tau; V_m)\right|\right) \tag{24}$$

and such that $z_e(x_h, \tau)$ appears to have spatial continuity over (x_h, τ). At this time, the identification of such reflection event surfaces is fundamentally subjective and interpretive. Let's define $x_c(\tau)$ ranging from $x_\alpha(\tau)$ to $x_\beta(\tau)$ such that

$$\phi_e(x_c(\tau), \tau) = \left\| z_e(x_c(\tau), \tau) - \overline{z}_e(\tau) \right\|_2 \tag{25}$$

and

$$\phi_e(x_c(\tau), \tau) < \delta\lambda_{\min}, x_c(\tau) \in \left[x_\alpha(\tau), x_\beta(\tau)\right], \tag{26}$$

where $\| \|_2$ denotes the L_2 norm, $\overline{z}_e(\tau)$ is the average over offset of $z_e(x_h, \tau)$

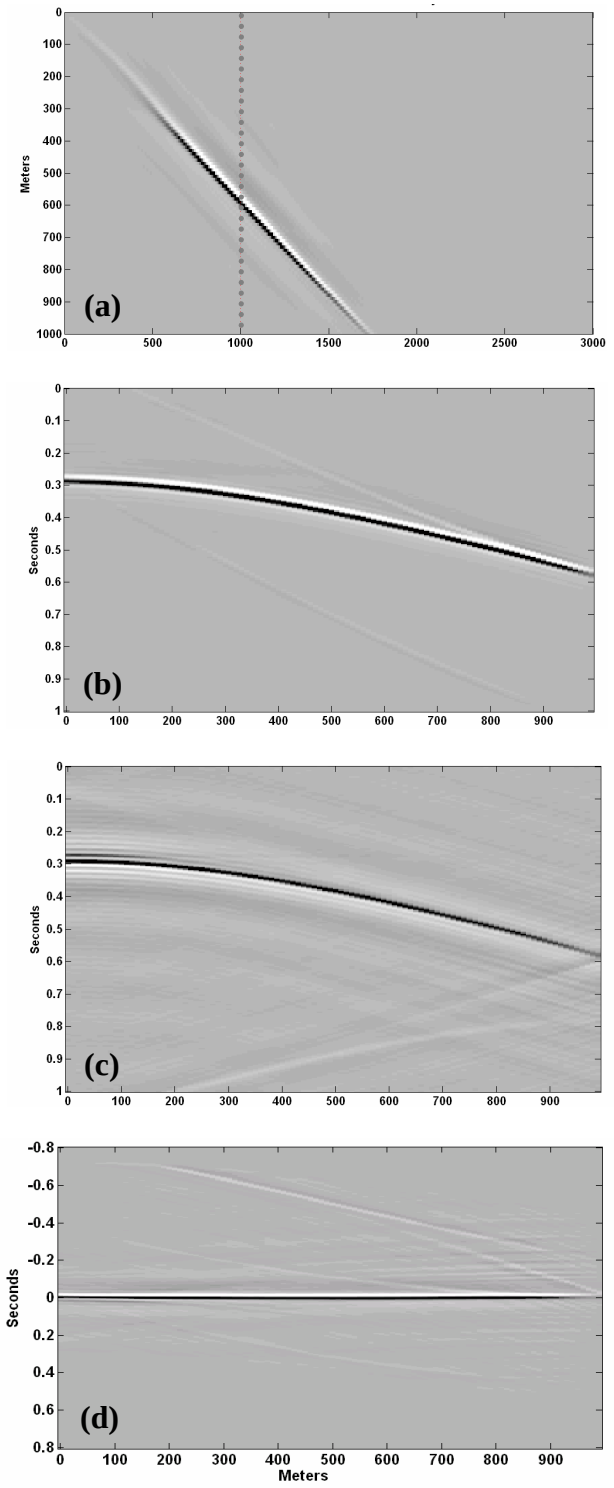

FIG. 1. Examples of CFP gathers where (a) shows the final stacked section migrated with $V_m = V$, for the location indicated by the dashed line in (a), (b) shows $u_i^- \left(x_h, t; V_m\right)$, (c) is the forward modeled downgoing wavefield $d_i^+ \left(x_h, t; V_m\right)$, and (d) shows a DTS panel, $G_{df} \left(x_h, x_o, z, \tau; V_m\right)$, where $z_r = 585$ m, $x_0 = 1000$ m, and *N*=100.

$$\overline{z}_e(\tau) = \text{mean}\left(z_e(x_h, \tau)\right), \tag{27}$$

δ is a dimensionless number greater than zero and $\lambda_{\min}$ as defined by equation (16). Then there exists a focusing scalar crosscorrelation lag, τ_f, that identifies the flattest part of $z_e\left(x_c\left(\tau_f\right), \tau\right)$ and the focusing depth z_f such that

$$x_c\left(\tau_f\right) = \max\left(x_f(\tau)\right), x_c\left(\tau_f\right) \in \left[x_\alpha\left(\tau_f\right), x_\beta\left(\tau_f\right)\right] \tag{28}$$

and

$$z_f = \overline{z}_e\left(\tau_f\right). \tag{29}$$

Thus z_f is the average depth of that part of $z_e(x_h, \tau)$ which is sufficiently flat. We say that V_m is correct to ε periods and δ wavelengths, and write this $V_m =_{\varepsilon,\delta} V$, at a position $\left(x_0, z_f\right)$ if there exists a nonnegative, dimensionless number $\varepsilon > 0$ such that

$$\left|\tau_f\right| f_{\max} < \varepsilon, \tag{30}$$

and

$$z_r =_{\varepsilon,\delta} z_f. \tag{31}$$

That is, the reflector and the focusing depths are equal.

■

The differences between the CFP and CICA approaches are two fold:

(1) For a particular reflection event, the CFP analysis starts with z_i, that is, an initial guess of the depth of the reflector while in the CICA approach, the analysis is done around the observed focusing depth, z_f, as defined by the flattest part of the event surface $z_e(x_h, \tau)$.

(2) In the CFP approach, at z_i, the offset-variant lag, $\tau_i(x_h) = t_{ui}(x_h) - t_{di}(x_h)$, depends on offset, x_h, whereas in the CICA, at z_f the focusing crosscorrelation lag, $\tau_f = t_{uf}\left(x_c\left(\tau_f\right)\right) - t_{df}\left(x_c\left(\tau_f\right)\right)$, is offset independent. Moreover, the CFP approach is an iterative approach that terminates when $\left|\tau_i(x_h)\right| f_{\max} < \varepsilon, \forall x_h \in \left[x_\alpha, x_\beta\right]$, in which case the depth-specific delay function becomes offset independent.

Consequently, the CICA approach should converge faster in approximating the true field than the CFP approach. However, the same updating procedure that is used in CFP will be used in CICA. So by splitting τ_f and applying half of it to the upgoing wavefield

and half to the downgoing wavefield, the true velocity can be approximated as we shall see later.

Furthermore, slicing $G_{df}\left(x_h, x_o, z, \tau; V_m\right)$ at different τ values produces the depth focusing gathers which can be assessed for flatness as in RCA. Also, the fact that energy focuses at a different depth than the true depth when $V_m \neq_{\varepsilon} V$ is a borrowed concept from DFA. So the CICA is a combination of the three previous methods.

Constant velocity medium

In a constant velocity medium, when the velocity used for migration $V_m =_{\varepsilon} V$, the event is imaged at the reflector depth, $z = z_r$. This also means that

$$\left|\left(t_d\left(x_h, x_0, z\right)\right) - \left(t_u\left(x_h, x_0, z\right)\right)\right| f_{\max} < \varepsilon, x_h \in \left[x_\alpha, x_\beta\right]. \tag{32}$$

It follows from the equation (32) and from the CICA hypothesis that $z =_{\delta} z_f$ and $\tau_f\ f_{\max} < \varepsilon$. There are numerous possible inversion schemes that could be used to invert for the true velocity from the updated traveltimes. In this report, we will use a simple inversion scheme in which the true velocity is estimated by fitting hyperbolae through the updated traveltimes. The traveltimes of the extrapolated wavefields at z_r can be calculated from

$$t_u\left(x_c\right) = \sqrt{{t_u}^2\left(x_c = 0\right) + \left(\frac{x_c}{V_m}\right)^2} \tag{33}$$

and

$$t_d\left(x_c\right) = \sqrt{{t_d}^2\left(x_c = 0\right) + \left(\frac{x_c}{V_m}\right)^2}\ , \tag{34}$$

where $x_c\left(\tau = 0\right) \in \left[x_\alpha\left(\tau = 0\right), x_\beta\left(\tau = 0\right)\right]$ (note the subscripts x_0 and z have been dropped from the notations of t_d and t_u) . Then the velocity can be solved for from either equation (33) or (34) since $V_m =_{\varepsilon} V$. However, when $V_m \neq_{\varepsilon} V$ the event is imaged at a depth that does not equal the reflector depth, that is, $z \neq z_r$ and also $t_d\left(x_h, x_0, z\right) \neq t_u\left(x_h, x_0, z\right)$. From the CICA imaging hypothesis, we can find τ_f and z_f. Then the true velocity, $\tilde{V}$, can be approximated by the following steps:

- Obtain an average estimate of the true velocity from the updated traveltime of the upgoing wavefield

$$V_u = \frac{\sum_{x_c(\tau_f)} \left(\sqrt{\frac{x_c{}^2(\tau_f)}{\left(t_u\left(x_c(\tau_f)\right) - \frac{\tau_f}{2}\right)^2 - \left(t_u\left(x_c(\tau_f)=0\right) - \frac{\tau_f}{2}\right)^2}} \right)}{|\alpha - \beta|}. \quad (35)$$

- Obtain an average estimate of the true velocity from the updated traveltime of the downgoing wavefield

$$V_d = \frac{\sum_{x_c(\tau_f)} \left(\sqrt{\frac{x_c{}^2(\tau_f)}{\left(t_d\left(x_c(\tau_f)\right) + \frac{\tau_f}{2}\right)^2 - \left(t_d\left(x_c(\tau_f)=0\right) + \frac{\tau_f}{2}\right)^2}} \right)}{|\alpha - \beta|}. \quad (36)$$

- Then $\tilde{V}$ can be found from

$$\tilde{V} = \frac{V_u + V_d}{2}. \quad (37)$$

Figures 2.a and 2.b show CICs when using $V_m =_{\varepsilon} V$ and $V_m \neq_{\varepsilon} V$, respectively. Note that the $G_{df}\left(x_h, x_o, z, \tau = 0; V_m\right)$ has a flat event in Figure 2.a and a frown in Figure 2.b. This also means that for $V_m = V$, $\tau_f =_{\varepsilon} 0$ and $z =_{\delta} z_r$. Figure 2.d shows that $G_{df}\left(x_h, x_o, z, \tau = \tau_f; V_m\right)$ has a flat event even though $G_{df}\left(x_h, x_o, z, \tau = 0; V_m\right)$ does not.

Next, we will use some numerical examples to show how the CICA hypothesis can be used to approximate the true velocity. Figure 3 shows composites of $t_u\left(x_c\left(\tau_f\right)\right)$ and $t_d\left(x_c\left(\tau_f\right)\right)$ of the upgoing and downgoing wavefields that are extrapolated to z_f using V_m for three cases: $V/V_m = 0.9091$ (Figure 3.a), $V/V_m = 0.8083$ (Figure 3.b), and $V/V_m = 0.7692$ (Figure 3.c). Two observations can be drawn from this example: (1) in the three cases, τ_f does not depend on offset and (2) even for a dipping reflector, the approximated velocity from the updated traveltimes has very small dip dependency.

Figure 4 sheds more light on the case $V/V_m = 0.8083$ by showing (a) the location of the analysis location on the stack section obtained with the true velocity, (b) traveltime from ray tracing, and (c) a composite of the upgoing wavefield, downgoing wavefield, and the travel time calculated using $\tilde{V}$. This example shows that the difference between the raytracing and hyperbola using $\tilde{V}$ traveltimes is small.

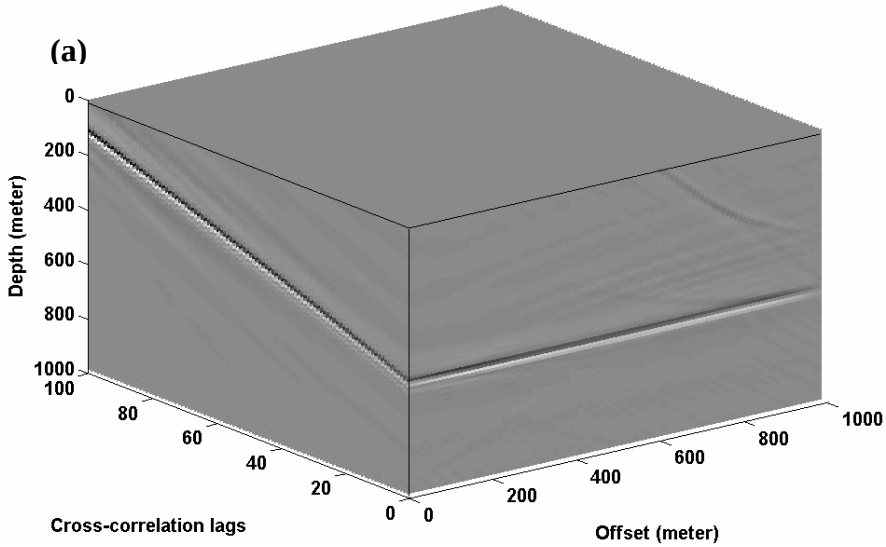
(a)
Depth (meter)
0
200
400
600
800
1000
100
80
60
40
20
0
Cross-correlation lags
0
200
400
600
800
1000
Offset (meter)

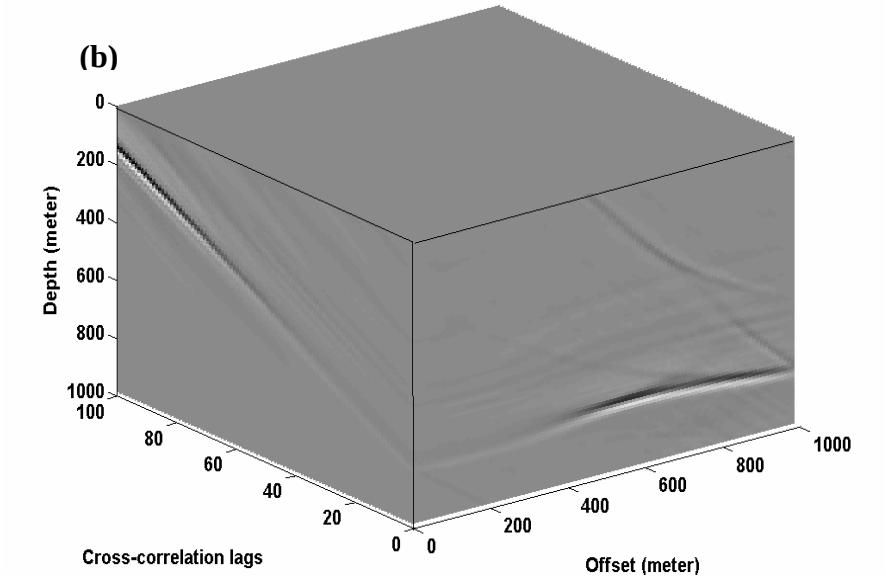
(b)
Depth (meter)
0
200
400
600
800
1000
100
80
60
40
20
0
Cross-correlation lags
0
200
400
600
800
1000
Offset (meter)

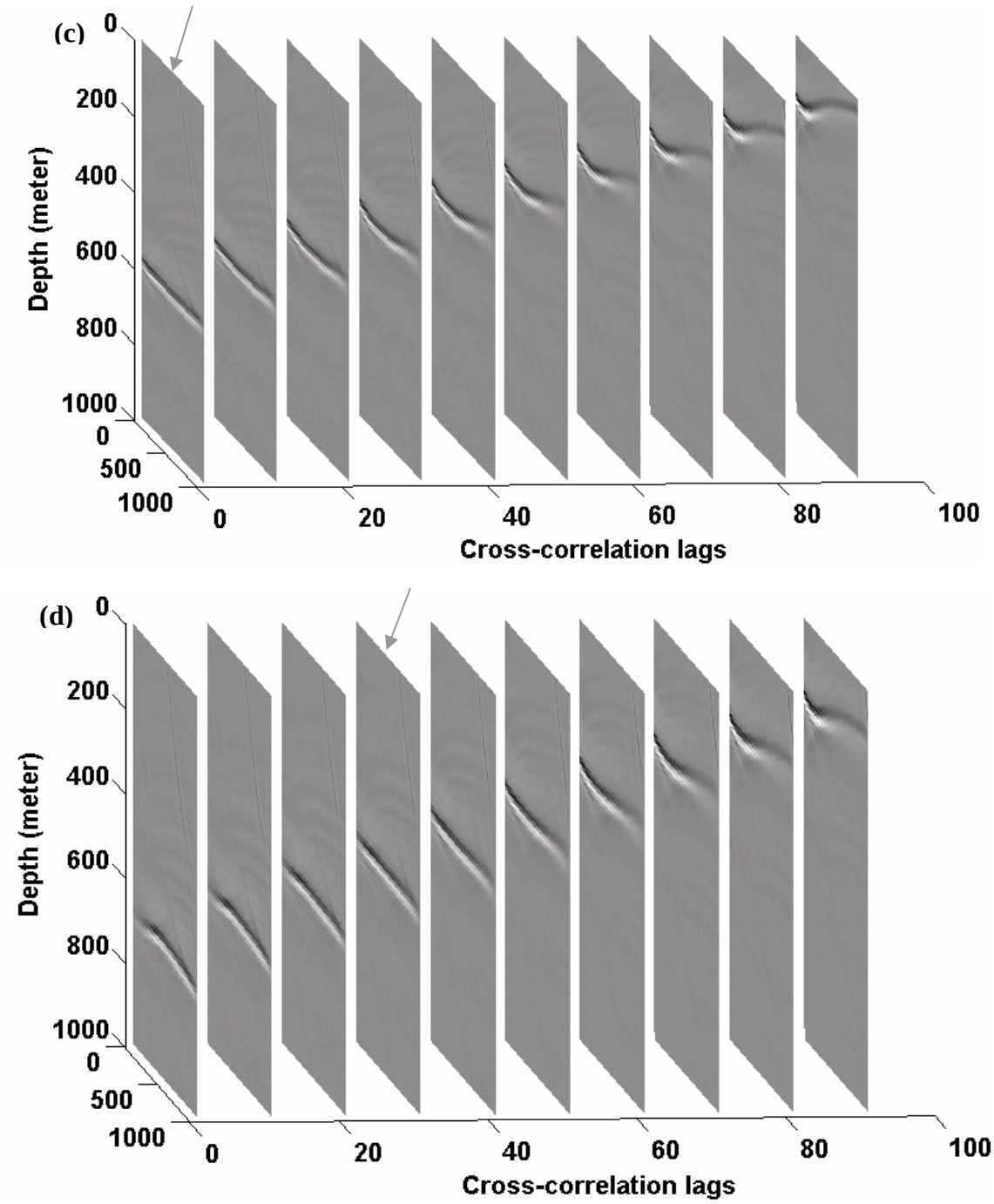

FIG. 2. (a) Common image cube (CIC) where (a) is obtained with $V_m =_{\varepsilon} V$ and (b) is obtained with $V_m > V$. Part (c) shows slices of the true velocity cube at different lags and (d) shows slices of the wrong velocity cube at different lags. The arrow indicates the location of $G_{df}\left(x_h, x_o, z = z_f, \tau = \tau_f, V_m\right)$.

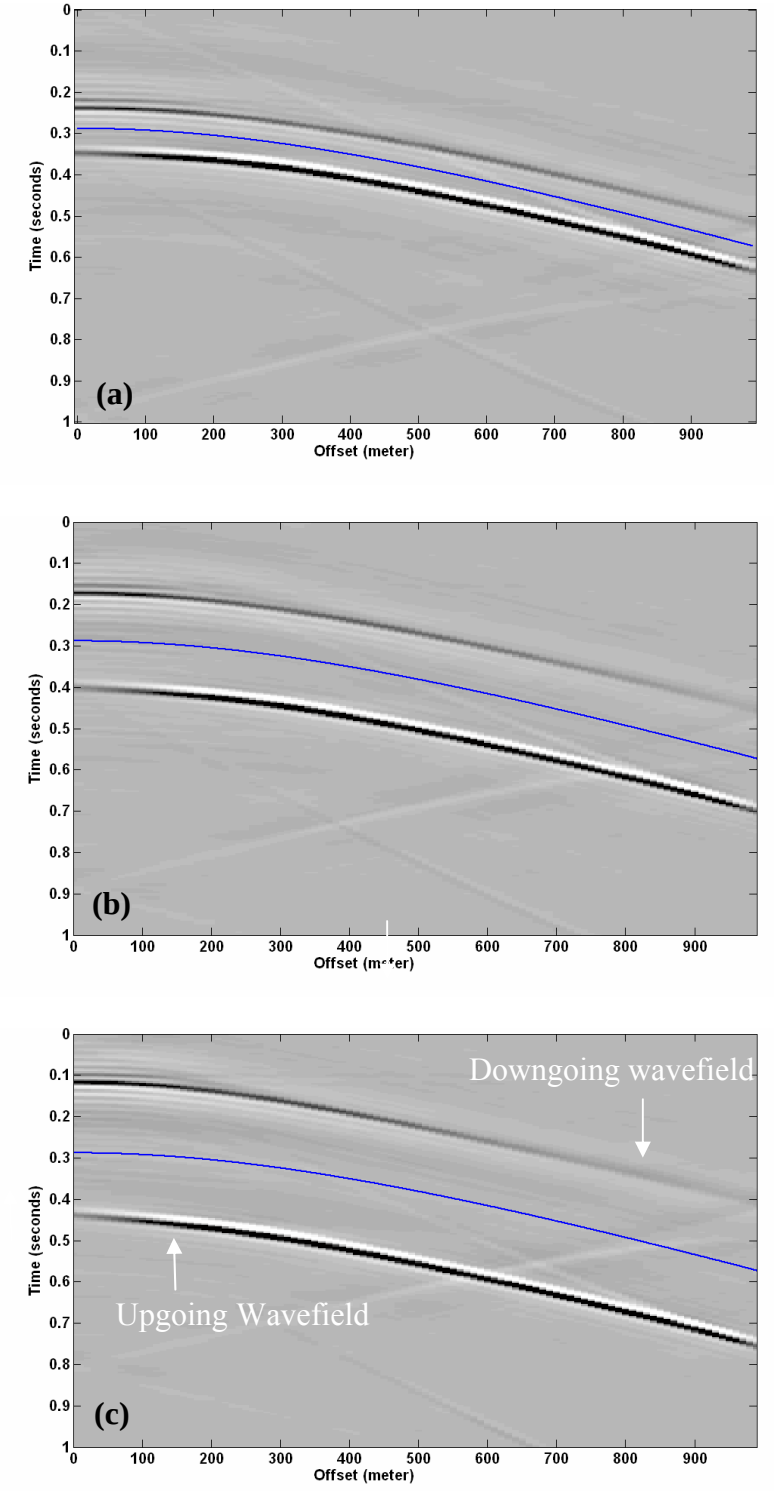

FIG. 3. Composite of the upgoing wavefield, downgoing wavefield, and ray tracing travel time with the true velocity where there is (a) 10% velocity error, (b) 20% velocity error, and (c) 30% velocity error.

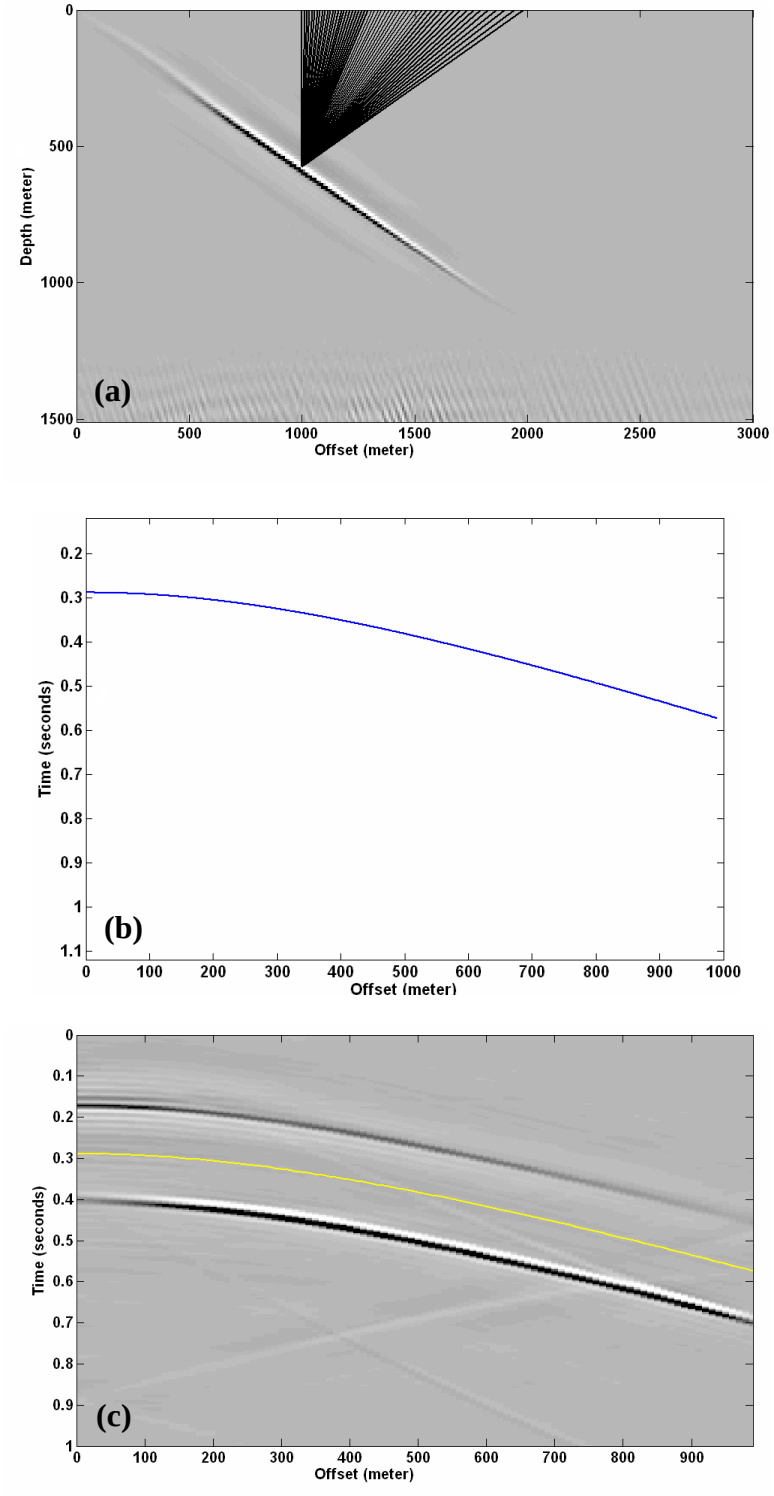

FIG. 4. (a) Stack section with the true velocity, (b) ray tracing travel time with the true velocity, and (c) a composite of the upgoing and downgoing wavefields for the 20% velocity error. The extrapolation depth of gathers in (c) is the focusing depth. The yellow curve is obtained using the estimated $\tilde{V}$.

Vertical Velocity variations

When the velocity varies with depth, the traveltime curve is only roughly a hyperbola. However, for small offsets, the root mean square (RMS) velocity is a good approximation to the average velocity (Yilmaz, 1987). Thus the same analogy that was used for the constant velocity case can be used here except that the velocity now is the RMS velocity instead of a constant.

Figure 5 shows numerical examples of using $V_m =_\delta V$ and $V_m \neq_\delta V$ for migration. For simplicity, all these models have only one event at a depth of 1000m. For the case in which $V_m =_\delta V$ (Figure 5.a), the $G_{df}\left(x_h, x = x_o, z = z_r, \tau = 0, V_m\right)$ has a flat event (Figures 5.c and 5.d). On the contrary, when $V_m \neq_\delta V$ (Figure 6.a), the $G_{df}\left(x_h, x = x_o, z = z_r, \tau = 0, V_m\right)$ does not have a flat event (Figures 6.b and 6.c). However, based on the CICA hypothesis, there exist τ_f and z_f such that $G_{df}\left(x_h, x = x_o, z = z_f, \tau = \tau_f, V_m\right)$ has a flat event. This common depth gather can be seen in Figure 6.c (indicated by an arrow). Figure 7 shows a composite of $t_u\left(x_h\right)$ and $t_d\left(x_h\right)$ at z_f, the travel time from ray tracing, and the travel time by using $\tilde{V}$ (the approximated RMS velocity from the analysis). This shows that for this model, the travel time from a hyperbolae using $\tilde{V}$ was a good approximation to the true travel time obtained from ray tracing.

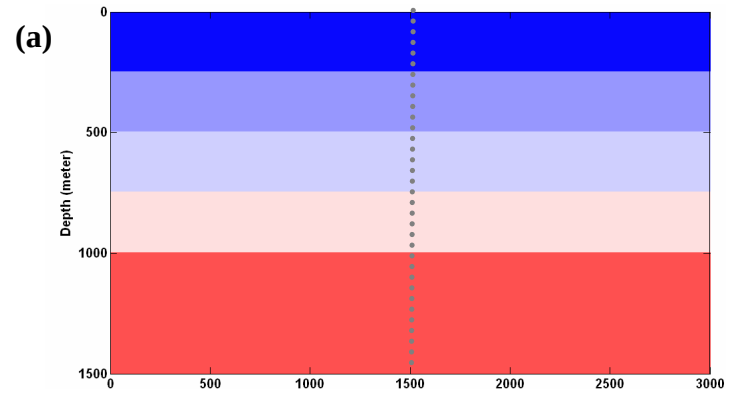
(a)
Depth (meter)
0
500
1000
1500
0
500
1000
1500
2000
2500
3000

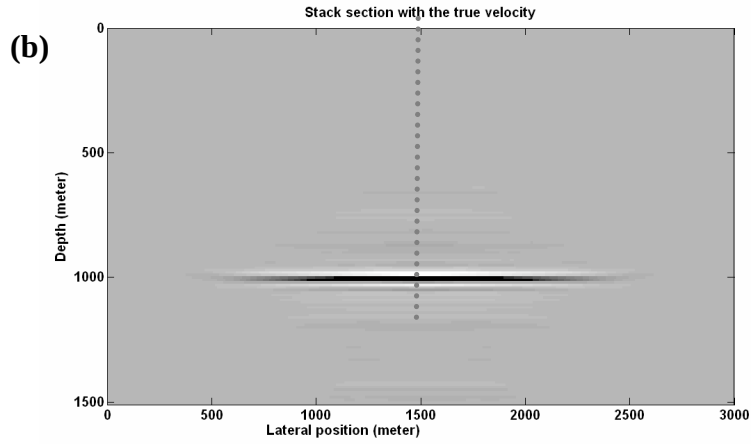
Stack section with the true velocity
(b)
Depth (meter)
0
500
1000
1500
0
500
1000
1500
2000
2500
3000
Lateral position (meter)

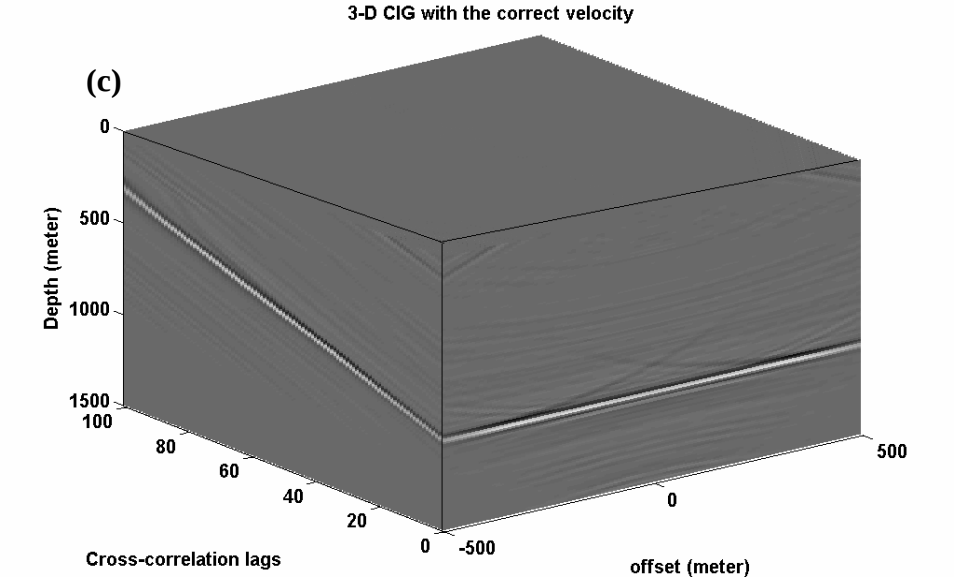
3-D CIG with the correct velocity
(c)
Depth (meter)
0
500
1000
1500
100
80
60
40
20
0
Cross-correlation lags
-500
0
500
offset (meter)

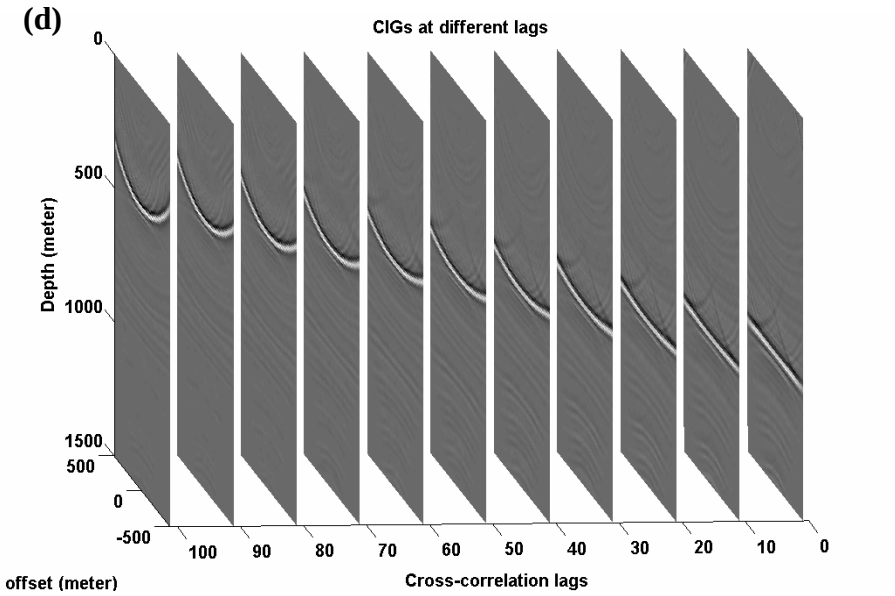

FIG. 5. Migration with $V_m =_\delta V$ where (a) shows the velocity model, (b) shows the final stack section obtained from $\sum_{x_h} G_{df}\left(x_h, x = x_o, z = z_r, \tau = 0; V_m\right)$, (c) shows the $G_{df}\left(x_h, x = x_o, z, \tau; V_m\right)$, and (d) shows slices of (c) for $x_o = 1500$ m.

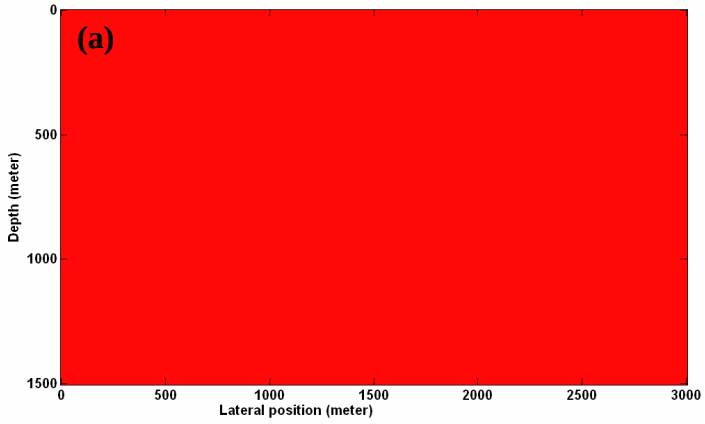

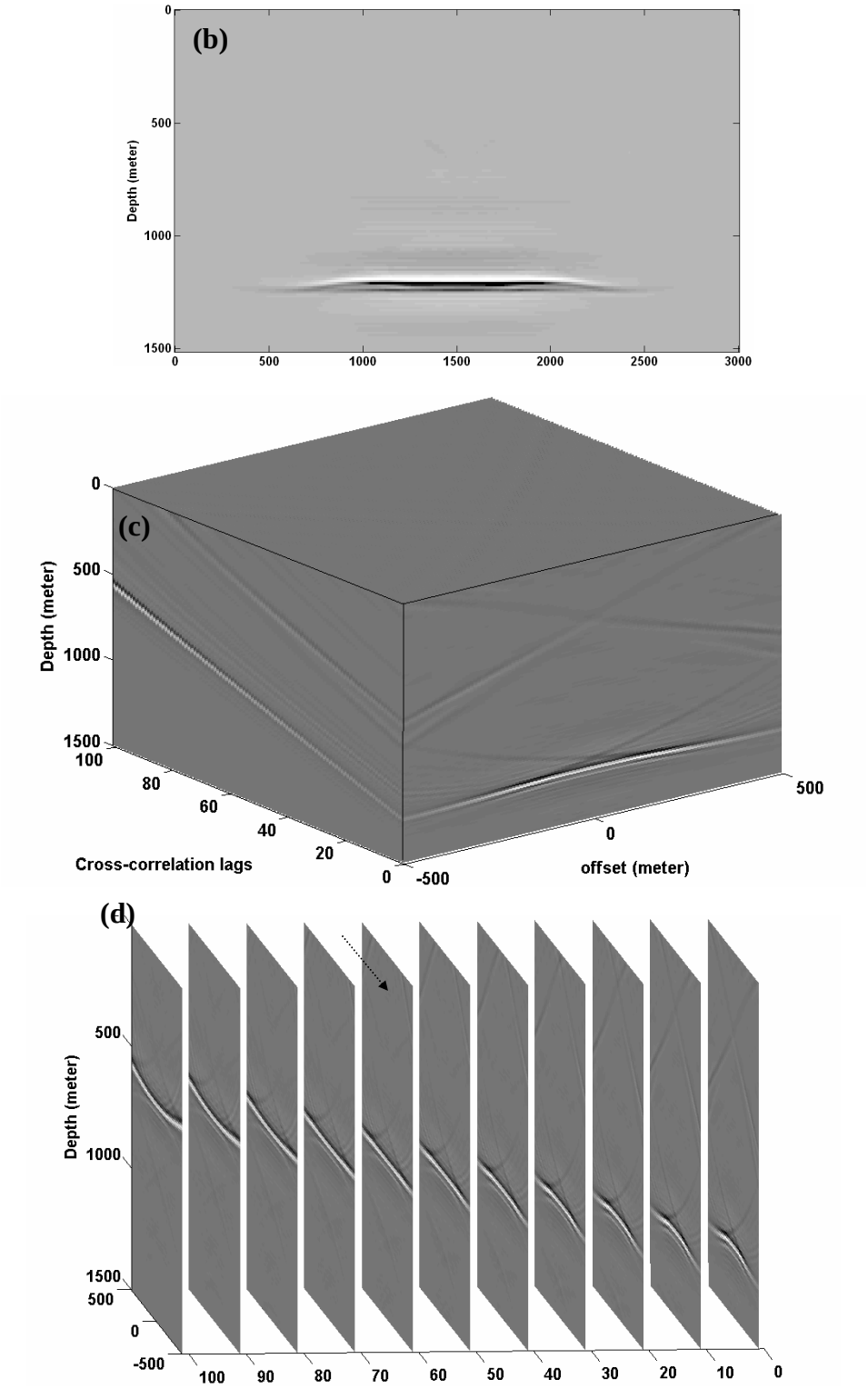

FIG. 6. Migration with $V_m \neq_\delta V$ where (a) shows the velocity model, (b) shows the final stack section obtained from $\sum_{x_h} G_{df}\left(x_h, x = x_o, z = z_r, \tau = 0; V_m\right)$, (c) shows the $G_{df}\left(x_h, x = x_o, z, \tau; V_m\right)$, and (d) shows slices of (c) for $x_o = 1500$.

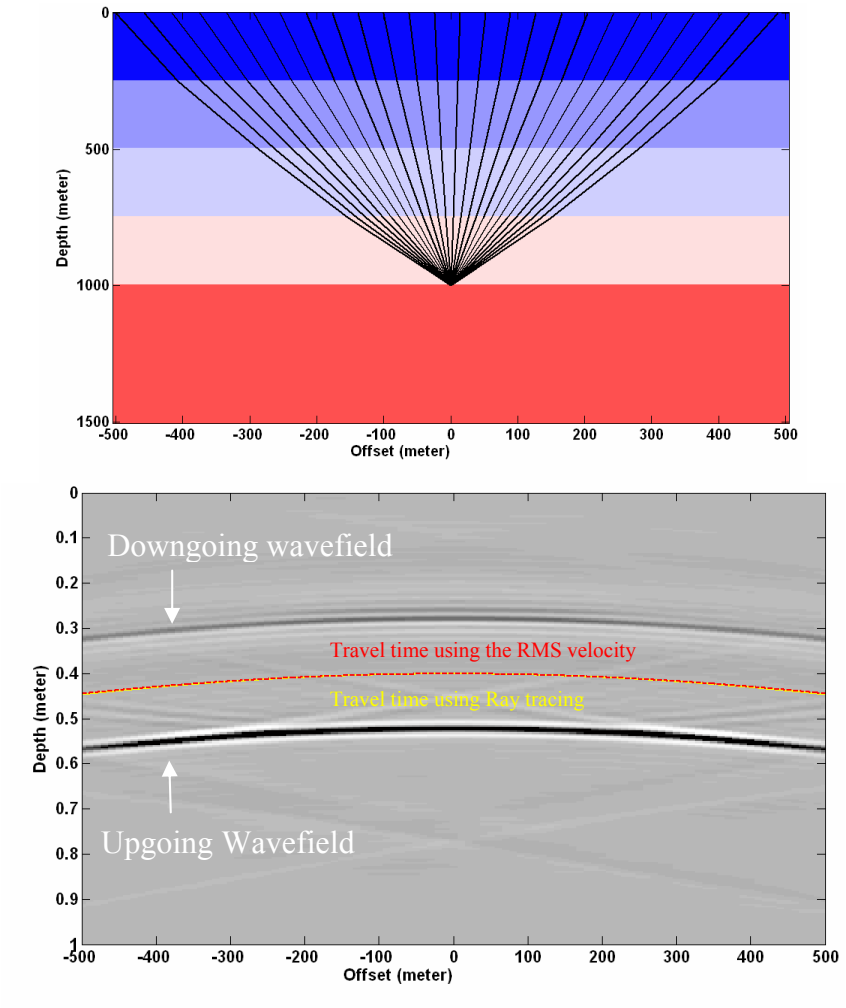

FIG. 7. Comparison of traveltimes of the ray-tracing and the hyperbola using the estimated velocity were (a) shows the ray-tracing at a lateral position, x_o, and (b) shows the traveltimes of the ray-tracing (yellow) and the hyperbola using the approximated RMS velocity. The extrapolation depth for the upgoing and downgoing wavefields is the focusing depth.

CONCLUSIONS

The numerical examples for the models of constant velocity and velocity varying with depth show that the CICA imaging hypothesis can be used to get an estimate of the true velocity when the background velocity model does not approximate the true velocity field. This method combines various aspects of RCA, DFA, and CFP methods. Further, it offers more prestack information than the other methods.

Even for a dipping reflector in a constant velocity medium, the current MVA methods might need a couple of iterations to get an accurate estimate of the true velocity. On the other hand, the CICA approach can achieve this on the first iteration. The CICA method is thus a promising technique for migration velocity analysis. The inversion formulas that are shown in this report might not yield accurate estimates of the velocities in the presence of complicated subsurface. In that case, global tomography should be used in instead.

REFERENCES

Al-Saleh, S. M., and Margrave, G. F., 2005, Enhancing the FOCI extrapolation method by using a weighted least-squares approach, This volume.

Al-Yahya, K., 1989, Velocity analysis by iterative profile migration: Geophysics, **54**, 718–729.

Berkhout, A. J., 1982, Seismic migration: Imaging of acoustic energy by wavefield extrapolation, A. Theoretical aspects, 2nd Ed.: Elsevier Science Publ. BV.

Berkhout, A. J., 1997a, Pushing the limits of seismic imaging, part I: Prestack migration in terms of double dynamic focusing: Geophysics, **62**, 937–953.

Berkhout, A. J., 1997b, Pushing the limits of seismic imaging, part II: Integration of prestack migration, velocity estimation, and AVO analysis: Geophysics, **62**, 954–969.

Berkhout, A. J., 2001, Seismic imaging beyond depth migration: Geophysics, **66**, 1895–1912.

Biondi, B., and Sava, P. , 1999, Wave-equation migration velocity analysis, 69th Annual International Meeting, SEG, Expanded Abstracts, 1723–1726.

Claerbout, J. F., 1976. Fundamentals of geophysical data processing: McGraw-Hill Book Co.

Claerbout, J. F., 1985, Imaging the earth's interior: Blackwell Scientific Publications, Inc

Clapp, R., and B. Biondi, 2000, Tau domain migration velocity analysis using angle CRP gathers and geologic constraints: 70th Annual International Meeting, SEG, 926–929.

de Bruin, C.G. M., C. P. A.Wapenaar, and A. J. Berkhout, 1990, Angle dependent reflectivity by means of prestack migration: Geophysics, **55**, 1223–1234.

Deregowski, S. M., 1990, Common offset migration and velocity analysis: First Break, **8**, 225–234.

Faye, J.P., and Jeannot, J.P., 1986, Prestack migration velocities from focusing depth analysis: 56th Ann. Internat. Mtg., Soc.Expl. Geophys., Expanded Abstracts, 438-440.

Gazdag, J., and Squazerro, P., 1984, Migration of seismic data by phase shift plus interpolation: Geophysics, **49**,124-131.

Hale, D., 1991, Stable explicit depth extrapolation of seismic wavefields: Geophysics, **56**, 1770-1777.

Holberg, O., 1988, Towards optimum one-way wave propagation: Geophys., Prosp., **36**, 99-114.

Lee, W. B., and Zhang, L., 1992, Residual shot profile migration: Geophysics, **57**, 812-822.

Liu, Z. and Bleistein, N., 1992, Velocity analysis by residual moveout: 1992 SEG expanded abstracts, p. 1034.

Liu, Z., and Bleistein, N., 1994, Velocity analysis by perturbation: 64th Ann. Internat. Mtg., Soc. Expl. Geophys., Expanded Abstracts, 1191–1194.

Lynn, W. S. and Claerbout, J. F., 1982, Velocity estimation in laterally varying media: Geophysics, **47**, 884-897.

MacKay, S., and Abma, R., 1993, Depth-focusing analysis using a wavefront-curvature criterion: Geophysics, **58**, 1148-1156.

Margrave, G. F. and Ferguson, R. J., 1999, Wavefield extrapolation by nonstationary phase shift: Geophysics, **64**, 1067-1078.

Margrave, G.F., Geiger, H.D., Al-Saleh, S., and Lamoureux, M.P., 2005, Improving explicit depth migration with a stabilizing Wiener filter and spatial resampling: submitted to Geophysics.

Varela, C. L., Stoffa, P. L., and Sen, M. K., 1998, Background velocity estimation using non-linear optimization for reflection tomography and migration misfit: Geophys. Prosp., 46, 51–78.

Yilmaz, O., and Chambers, R., 1984, Migration velocity analysis by wavefield extrapolation: Geophysics, **49**, 1664–1674.

Yilmaz, O., Seismic Data Processing, 1987, Society of Exploration Geophysicists.

Zhu, J., Lines, L., and Gray, S., 1998, Smiles and frowns in migration/velocity analysis: Geophysics, **63**, 1200-1209.